Supplementary Information for

Global electronic reconstruction at the atomically smooth, polar (111)-oriented oxide interface

S. Ryu[1], H. Zhou[2], T.R. Paudel[3], N. Campbell[4], J. Podkaminer[1], C. W. Bark[1], T. Hernandez[4], D. D. Fong[5], Y. Zhang[6], L. Xie[6], X. Q. Pan[6,7], E. Y. Tsymbal[4], M. S. Rzchowski[3], and C. B. Eom[1*]

[1] Department of Materials Science and Engineering, University of Wisconsin, Madison, Wisconsin 53706, USA.
[2] X-ray Science Division, Argonne National Laboratory, Argonne, Illinois 60439, USA.
[3] Department of Physics and Astronomy, University of Nebraska, Lincoln, Nebraska 68588, USA.
[4] Department of Physics, University of Wisconsin, Madison, Wisconsin 53706, USA.
[5] Materials Science Division, Argonne National Laboratory, Argonne, Illinois 60439, USA.
[6] Department of Materials Science and Engineering, University of Michigan, Ann Arbor, Michigan 48109, USA.
[7] Department of Materials Science and Engineering, University of California, Irvine, California 92697 USA.

1. Structure and charge density in the 111 orientation

As seen in the Figure S1, a hexagonal lattice along [111] direction can be defined in the frame of a cubic perovskite lattice. Charge per unit area of LAO and STO is $\pm 3e/\sqrt{3}a^2$ and $\pm 4e/\sqrt{3}a^2$, respectively. The equivalent surface charge densities are $\pm 1.5e/\sqrt{3}a^2$ and $\pm 2e/\sqrt{3}a^2$, respectively.

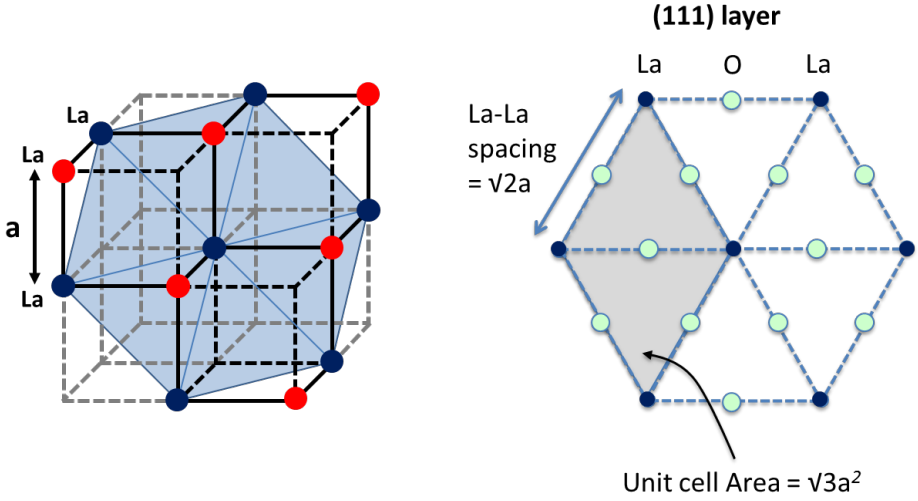

Figure S1. The definition of a hexagonal lattice in an ABO_3 cubic perovskite lattice and resultant unit cell area.

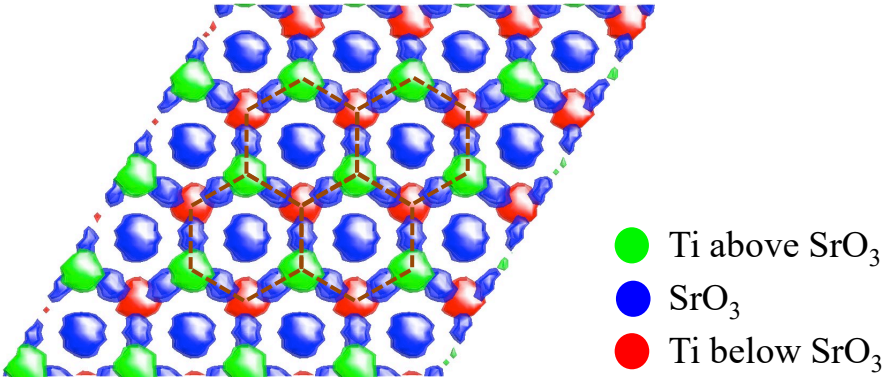

Figure S2. The projection of the three-dimensional electron density isosurface map along [111] direction for $SrTiO_3$ (111) system experimentally determined by surface X-ray diffraction and the COBRA method. One SrO_3 atomic layer together with two adjacent Ti atomic layers is overlaid in this projection view. The bigger isosurface blue blob in the center of a honeycomb lattice represents a Sr atom. The smaller blue blob at the middle of the edge of a honeycomb lattice represents an oxygen atom.

Theoretical modeling. First-principles calculations were performed using density functional theory (DFT) as implemented within the Vienna ab initio simulation package (VASP). The projected augmented wave (PAW) method was used to approximate the electron-ion potential, and the local density approximation (LDA) was used to include exchange and correlation effects. LAO/STO (111) interfaces were constructed using a supercell geometry where n-

bilayer of LAO (n = 5, 6, 8, 9 and 16) is placed on top of m-bilayer of STO (m = 3), both stacked in the [111] direction, and a 1.5 nm vacuum layer separates the LAO/STO structure. Instead of the exact surface reconstruction that should occur, we assumed particular kind of surface reconstruction, which is LaO3-AlO instead of pristine LaO3-Al. This will affect the relaxation of surface layers in rather artificial way. We hence removed those data points affected by this particular choice for the experimental comparison. 3 bilayers and 5 bilayers show similar relaxation patterns with insulating interfaces. We also assumed that the interface was LaO_3/Ti following our COBRA results. Constructed in such a way stoichiometric supercell contains a polar bottom surface of STO terminated by a $(SrO_3)^{4-}$ monolayer and thus produces an electric field in STO. To eliminate this unphysical field we removed an O atom to form a $(SrO_2)^{2-}$ monolayer and thus a non-polar bottom surface of STO. To preserve stoichiometry of the system we put this O atom to the top monolayer of LAO to create an AlO monolayer on the surface, resulting in the stacking sequence of $AlO/LaO_3/Al/LaO_3/\ldots/Al/LaO_3/Ti/SrO_2/Ti/SrO_3/\ldots/Ti/SrO_2$. The in-plane lattice constant of the superlattice was fixed to be the calculated bulk lattice constant of STO, i.e. a = 3.864 Å. To avoid an unphysical electric field in vacuum due to periodic boundary conditions of the supercell calculations a dipole layer was introduced in vacuum to cancel this field. In the calculation, we used a kinetic energy cutoff of 340 eV for the plane wave expansion of the PAWs and an equally spaced mesh of 4×3×1 k points in the $[1\bar{1}0]$, $[11\bar{2}]$, and [001] directions, respectively, for Brillouin zone integration. All the ionic positions were relaxed until the atomic forces were less than 0.01 eV/Å.

Fabrication of LAO/STO (111) heterostructures. All the LAO films were grown by pulsed-laser-deposition at 550 °C under PO_2 of 10^{-3} mbar. Before deposition, STO substrates were soaked in de-ionized water for 30 mins and chemically etched with buffered hydrofluoric acid for 1 min, and then annealed at 1000 °C for 6 hours in oxygen flow.

Transport measurements. We utilized direct ultrasonic wire bonding method to make electrode contacts at the interface for the transport measurements. Immediately after the film growth was completed, the heterostructures were mounted on chip carriers and aluminum wires were bonded at each corner or electrode pad of Hall bar patterns by using West Bond wedge bonder. Chip carriers were transferred to a cryostat and then stabilized in the dark environment to remove any photon-induced charge carrier. Additional measurements were made with patterns in a Hall geometry, giving confirmative results.

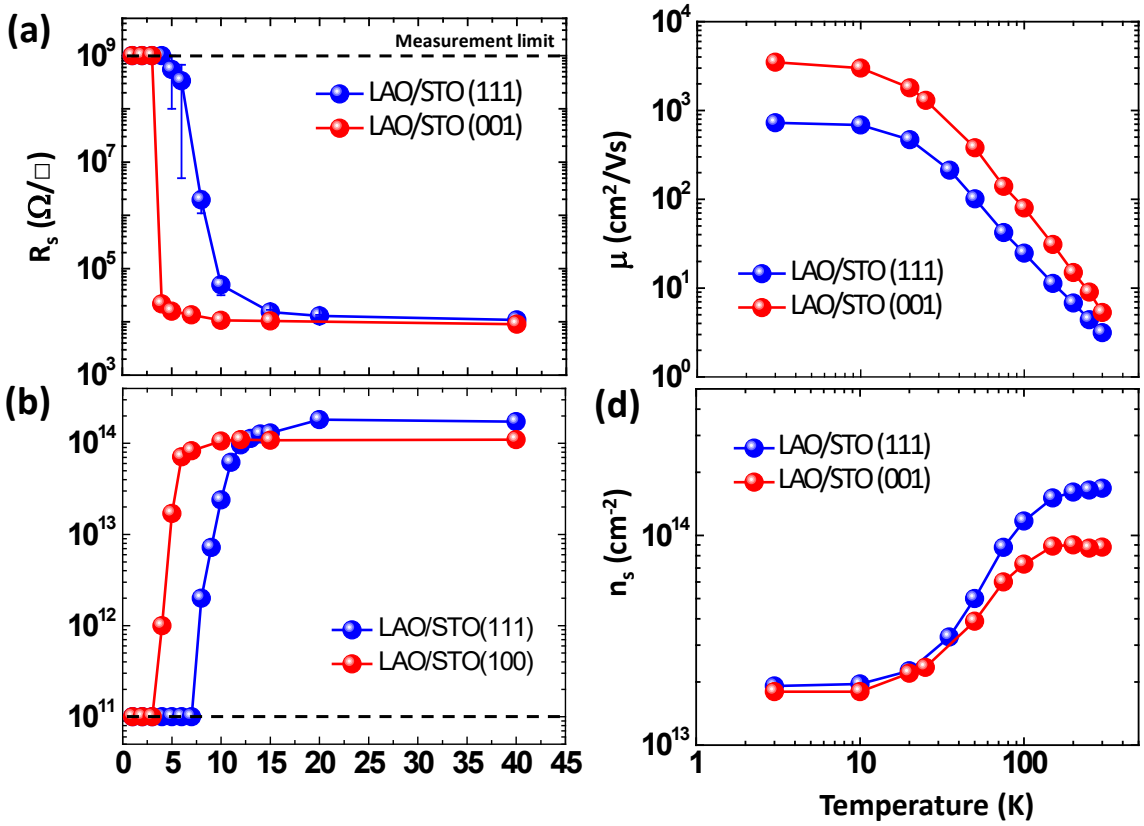

Figure S3: Influence of the LAO film thickness on two-dimensional transport properties at the LAO/STO (111) interface. (a) Sheet resistance and (b) carrier concentration as a function of the number of bilayers. It shows a broad transition compared to the LAO/STO (001) interface. (c) Mobility and (d) carrier concentration of the 20 bilayer LAO film as a function of temperature.

2. X-ray Surface Diffraction and COherent Bragg Rod Analysis (COBRA). The atomic structure of LAO/STO (111) heterostructures was investigated at beamline 12-ID-D of the Advanced Photon Source by measuring the diffraction intensities along the substrate-defined symmetry non-equivalent crystal truncation rods (CTRs). The measurements were carried out on a six-circle Huber goniometer, using an x-ray energy of 16 keV (λ = 0.7749 Å). The x-ray beam with a profile of 40 μm (vertical) × 500 μm (horizontal) has a flux of 1×10^{12} photons/sec. The two-dimensional scattering images of CTRs at each step in the reciprocal lattice unit were recorded by using a pixel array area detector (Dectris PILATUS 100 K). The L-scans along the specular CTRs were obtained by properly removing the background scattering contributions using the area detector images. Subsequently, COBRA was used to extract the three-dimensional electron density profile and layer-integrated electron densities along the [111] direction, from which it allows us to determine atomic positions as well as to estimate layer occupancy and stoichiometry. In general, COBRA is an x-ray phase-retrieval method which uses the fact that the complex structure factors (CSFs) vary continuously along the CTR to determine the diffraction phases from the measured diffraction intensities. The CSFs are then Fourier transformed into real space to obtain the electron density profile of the film and of the substrate with sub-Ångstrom resolution.

2. COherent Bragg Rod Analysis (COBRA) on LAO/STO (111) heterointerfaces.

The experimental data of representative crystal truncation rods (CTRs) for the 3-bilayer (insulating) and the 20-bilayer (conducting) heterostructures are shown in Figure S4. All the CTR measurements have been carried out at the energy of 16.0 keV. The diffraction intensity along the rods (excluding the Bragg peaks) varies by more than four orders of magnitude with excellent signal-to-noise ratio. The intensity modulations associated with Laue thickness fringes between each Bragg peak indicate the coherence of LAO thin film on STO substrate and contain the complete structural information across the interfacial region including the film and the top unit cells of the substrate. COBRA is the most effective technique to retrieve the full atomic structures from one unit-cell layer to another for epitaxial thin films that are just a few unit cells thick, which is otherwise inapplicable by using the standard x-ray diffraction analysis algorithms. The reference structures chosen as the starting point for the COBRA analysis were the bulk STO (111) substrate with the nominal (bulk) LAO unit cell layers. In our phase retrieval approach, the topmost four unit cells along the (111) direction were allowed to deform. Those top unit cell layers of the substrate turn out to have subtle structural modifications but critical to the physical properties of the heterointerfaces. As seen in Figure S5, the final calculated and measured structure factors are in very good agreement. Similar agreement was found for all other symmetry non-equivalent CTRs and the overall x-ray reliability factor is about 4-6%.

The integrated electron numbers as a function of Z Height for respective atomic layers, deduced from the density profiles, are demonstrated in Figure S5. A relatively sharp interface between LAO (111) layers and STO (111) substrate can be discerned explicitly from both figures. Both 3 bilayer and 20 bilayer films have a similar interfacial width of around 1 nm, which is as narrow as that obtained in the best cases of the LAO/STO (001) system. Note also that the insulating 3 bilayer film has 4^{th} bilayer on top with incomplete coverage. This incomplete coverage for the last few bilayers is also found in 20 bilayer conducting film. This indicates that the total film thickness can vary by a few bilayers from the controlled nominal thickness.

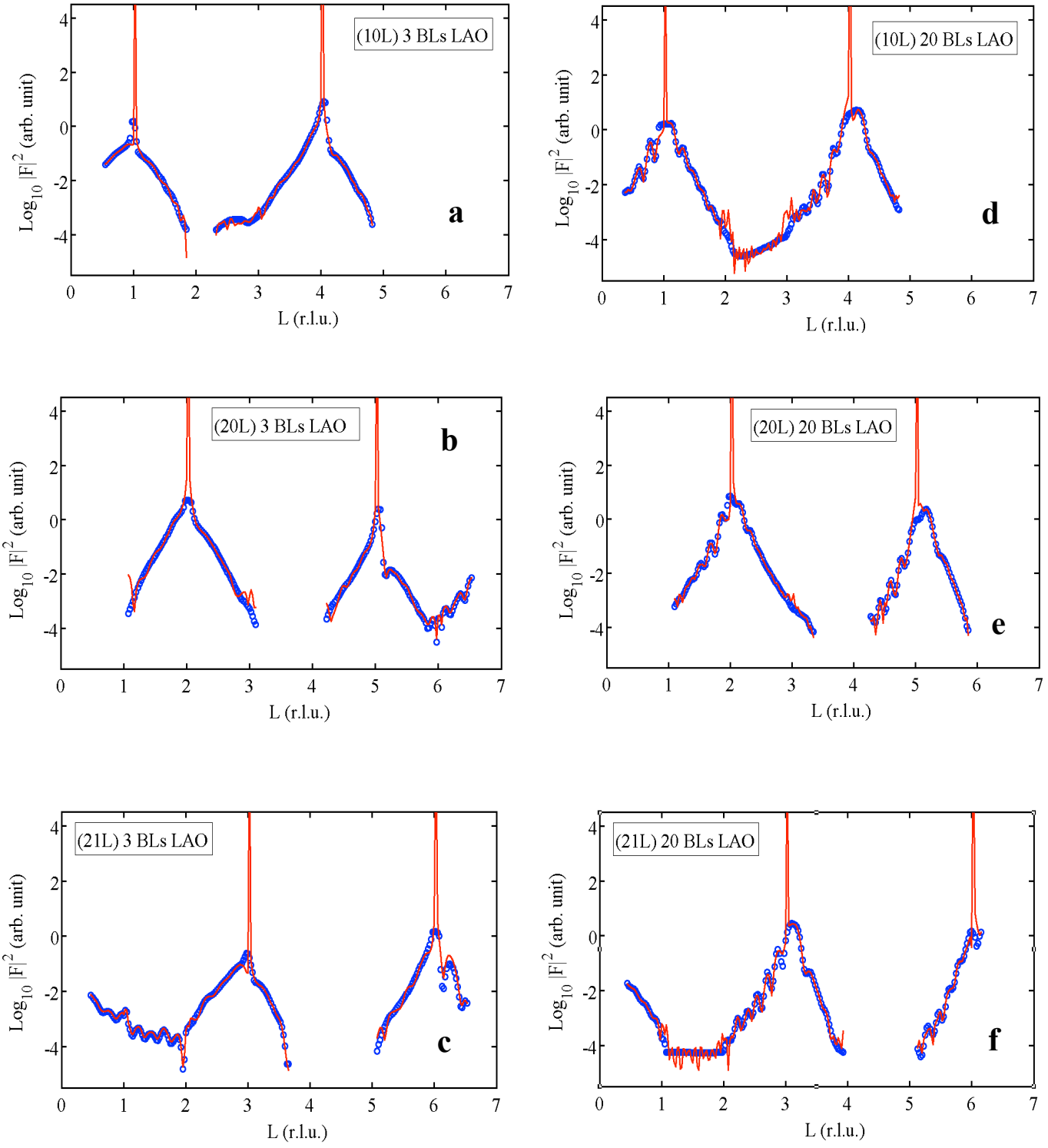

Figure S4. Representative measured (blue circles) and calculated (red lines) crystal truncation rods of (a-c) LAO 3 bilayers and (d-f) LAO 20 bilayers heterostructures. The scattering signals in some mid-zones between two substrate defined Bragg peaks are too weak (way much below the noise level) to be collected in the measurements.

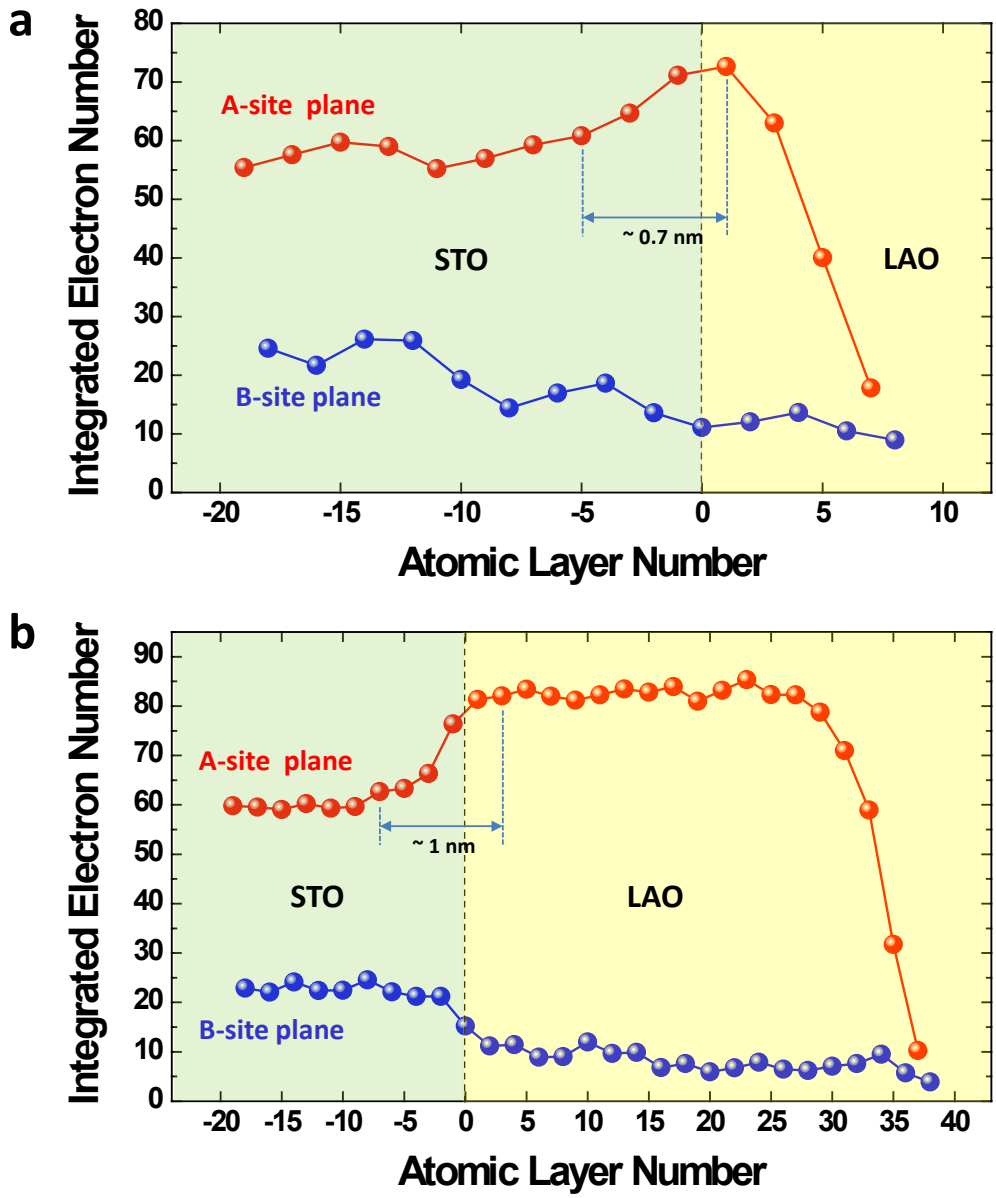

Figure S5. Integrated electron number of the 3 bilayers (a) and 20 bilayers of LAO (b), respectively, as a function of Z height. The interfacial width of AO_3 plane for each sample is marked in the figure. Intensity drops near the top surface of LAO films mean the incomplete coverage and are led to the thickness variation with respect to the nominal thickness.

3. Modification of the top surface of the treated STO (111) substrate.

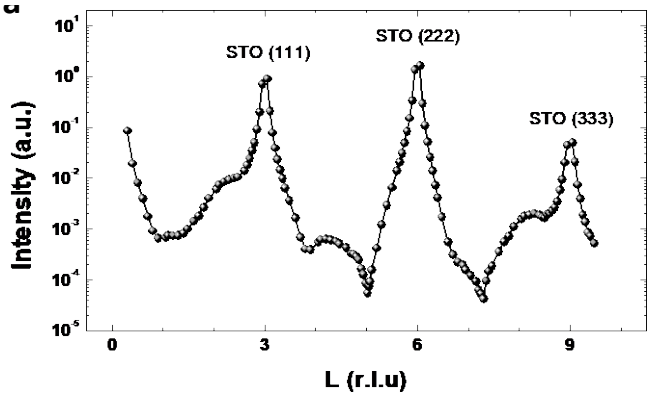

Figure S6. (a) Specular CTR (00L) of a treated $SrTiO_3$ bare substrate. The bare STO (111) surface shows non-trivial CTR intensity variations (significant bumps in Fig. S2(a)) between Bragg peaks which should not appear without surface reconstruction.

In this study, an atomically smooth STO (111) surface with step and terrace structures was obtained by chemical etching (standard buffered HF) and further thermal annealing (1000°C in oxygen rich environment for a few hours).

4. Theoretical calculation of AO_3-AO_3 interlayer spacing and B-site off-center displacement.

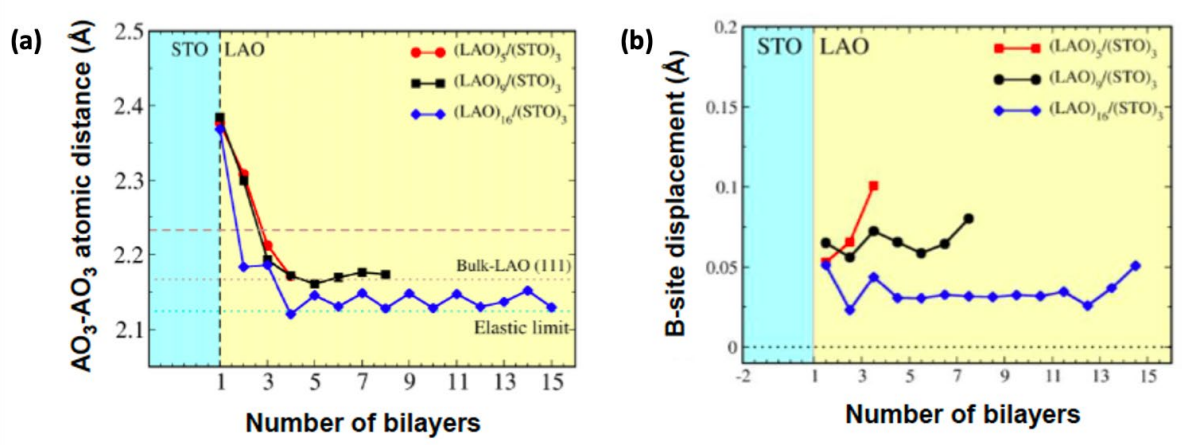

Figure S7. (**a**) AO_3-AO_3 interlayer distance and (**b**) B-site off-center displacement for different LAO thickness n in $(LAO)_n/(STO)_3$ heterostructures obtained from DFT calculations. Two top mono layers are not shown.

It is seen that the interlayer distance decreases with LAO thickness due to decreasing electric field in LAO. At a large LAO thickness it saturates at a value corresponding to the elastic limit as determined by the in-plain strain. The off-center displacement remains positive and also decreases with LAO thickness due to decreasing electric field in LAO.